

SLAC-PUB-5943
SCIPP 92/56
October 30, 2018

Hydrodynamic Stability Analysis of Burning Bubbles in Electroweak Theory and in QCD[★]

PATRICK HUET

*Stanford Linear Accelerator Center
Stanford University, Stanford, CA 94309*

KEIJO KAJANTIE

*Department of Theoretical Physics, University of Helsinki
Siltavuorenpenneri 20 C, 00170 Helsinki, Finland*

ROBERT G. LEIGH

*Santa Cruz Institute for Particle Physics
University of California, Santa Cruz, CA 95064*

BAO-HUA LIU AND L. MCLERRAN

*Theoretical Physics Institute
School of Physics and Astronomy, 116 Church St. S. E.
University of Minnesota, Minneapolis, MN 55455*

★ Research supported by the Department of Energy under grants DE-AC03-76SF00515 and DE-FG03-92ER40689 and by the National Science Foundation under grant PHY89-04035.

ABSTRACT

Assuming that the electroweak and QCD phase transitions are first order, upon supercooling, bubbles of the new phase appear. These bubbles grow to macroscopic sizes compared to the natural scales associated with the Compton wavelengths of particle excitations. They propagate by burning the old phase into the new phase at the surface of the bubble. We study the hydrodynamic stability of the burning and find that for the velocities of interest for cosmology in the electroweak phase transition, the shape of the bubble wall is stable under hydrodynamic perturbations. Bubbles formed in the cosmological QCD phase transition are found to be a borderline case between stability and instability.

1. Introduction

There is renewed interest in the dynamics of the electroweak phase transition [1 - 4]. This is due in part to the possibility that the baryon asymmetry of the universe might be generated at such a transition [5-9]. If the phase transition is first order then all of the conditions necessary for generating a baryon excess are present in the electroweak theory and its generalizations.

The Sakharov conditions for generating a baryon number excess are [10]:

1. Baryon Number Violation
2. CP Violation
3. Lack of Thermodynamic Equilibrium

The first condition is now well established in electroweak theory [11-16]. The rate of baryon number violation at temperatures larger than $T \geq 100$ GeV is known to be much greater than the expansion rate of the universe, and not much less than a typical particle scattering time.

The second condition is satisfied in the standard model, although explicit calculations show that the effects associated with CP violation arising from the quark mass matrix is much too small to generate an acceptably large baryon asymmetry. This is straightforward to patch up in generalizations of the standard model by allowing CP violation in the scalar interactions in an extended Higgs sector.

The third condition is satisfied if the electroweak phase transition is first order. The transition to the ordered low temperature phase takes place by bubble nucleation. Since all of the old phase must pass through the walls of a bubble where the matter is strongly out of thermal equilibrium, *all* of the matter is strongly out of equilibrium at some time during the phase transition. If the baryon asymmetry is made near or at the bubble walls, then all of the Sakharov conditions can be satisfied.

The electroweak phase transition is believed to be of first order. This has been shown to be true to the first few orders in perturbation theory [2-4]. In higher

orders, if α_W is small enough, then these calculations are reliable. For realistic values of $\alpha_W \sim 1/30$, these results are somewhat controversial, and perhaps may only be definitely resolved using non-perturbative lattice methods. In this paper we will assume that the electroweak phase transition is of first order, and will accept at face value the results of perturbative computations.

If the QCD hadronization phase transition is of first order, there might be consequences in both cosmology and heavy ion collisions. Whether or not the transition is first order is the subject of much study using lattice non-perturbative methods [17]. The order of the transition depends sensitively on the number of quark flavors and the quark masses and the physical case seems to be at the borderline between first and second order transitions [18]. In the following, we shall assume that the QCD phase transition is first order.

To proceed with a semi-quantitative analysis of the effects of a first order phase transition either in cosmology or during a heavy ion collision, one needs to understand the formation and growth of phase transition bubbles. For the electroweak and QCD cases, much is now known [19-25]. In particular, the limiting velocity of such walls has been computed for electroweak theory, and the shape of the wall near the burning surface is known. In the QCD case, the macroscopic features of the bubbles have been studied.

In this paper, we discuss the hydrodynamic stability of the bubble propagation. This has been discussed previously for the QCD phase transition [26]. We find however that the previous analysis was incomplete. If this analysis is applied to either QCD or electroweak theory, one would conclude that whenever the wall velocity is less than the sound velocity of the matter, then the bubble wall propagation is unstable. Our results are in contradiction with these conclusions. The source of the discrepancy is a more thorough treatment of the boundary conditions for the motion of the bubble wall.

The outline of this paper is the following. In the second section of this paper, we derive the macroscopic features of phase transition bubbles for the electroweak

phase in the 1+1 dimensional approximation, extending known results for the case of QCD [20-21]. In the third section, we derive the equations which describe a possible convective instability which could affect bubble wall propagation. Our analysis is fully relativistic, but we also discuss the non-relativistic limit. We point out the origin of the discrepancy between our results and those which have been previously derived. In the fourth section, we solve for the possible instability for the electroweak and QCD transitions. For the electroweak theory, we find stable growth for all velocities larger than $\sqrt{\alpha_W/2\pi} \sim 0.07$. Detailed computations [23,24] of velocities favor $v > 0.1$, and so this instability is of no physical interest. For the quark-hadron phase transition, our analysis is inconclusive. A conclusive statement can be made only after the relevant parameters of the phase transition are known more accurately. In the last section, we summarize our results.

2. Macroscopic Bubble Features

Suppose we have a system which has a first order phase transition at a temperature T_c . If the system is expanding, then the system supercools below T_c before nucleating droplets of the low temperature phase. After these droplets have formed, they begin to grow and expand into the system. If the supercooling is sufficiently strong, as is the case in the electroweak phase transition, then the droplets expand until they collide with one another and complete the phase transition. If the supercooling is sufficiently weak, as is the case in the QCD phase transition in cosmology, then the droplets expand until there is a mixed phase of droplets of the low temperature phase embedded within the high temperature phase. The subsequent evolution of the mixed phase involves coalescence of droplets, and as the system expands, an increase in the volume of the low temperature phase at a rate determined only by the rate of expansion of the system. Eventually, all of the system falls into the low temperature phase when expansion has reduced the energy density of the system to that of the low temperature phase.

In either case, for some time after nucleation, the bubbles freely expand into the system eating up the high temperature phase. If the growth of the bubbles

is hydrodynamically stable, then we expect that the bubble shape is smooth over macroscopic distances and should be spherical. The microscopic physics is only important in a region of order the diffusion length, a typical particle mean free path, near the surface of the bubble wall. This is seen explicitly in the hydrodynamic equations, which admit similarity solutions, that is, where the typical size scale is proportional to the time [20].

The analysis of a realistic situation is however a little complicated. There are two cases one must distinguish, referred to as *deflagrations* and *detonations*.

A detonation occurs when the velocity of the burning front is larger than the sound velocity of the matter in the high temperature phase. This turns out to be equivalent to the case when in the rest frame of the burning front, the velocity of matter behind the burning front is less than that in front of it.

This burning front in its rest frame is shown in Fig. 1. This is a frame which we will use for analyzing possible convective instabilities. For understanding the physics, it is sometimes more useful to consider the reference frame where the bubble wall moves, but the matter far in front of it is at rest.

For the single front shown in Fig. 2 we have four unknowns, all other thermodynamic quantities follow from the equation of state, $p = p(T)$, $s = p'(T)$, $\epsilon(T) = Ts(T) - p(T)$. We shall neglect all chemical potentials. Between the four unknowns, two equations follow from conservation of energy and momentum fluxes. By requiring that $\partial_\mu \Theta^{\mu\nu} = 0$ with^{*} $\Theta^{\mu\nu} = (\epsilon + p)u^\mu u^\nu - pg^{\mu\nu}$, it follows that $\Delta\Theta^{\mu z} = 0$, where z is the direction of motion of the bubble wall. From these one can, for instance, solve for the two velocities in terms of the two temperatures as

$$v_h^2 = \frac{(p_h - p_q)(\epsilon_q + p_h)}{(\epsilon_h - \epsilon_q)(\epsilon_h + p_q)}, \quad v_q^2 = \frac{(p_q - p_h)(\epsilon_h + p_q)}{(\epsilon_q - \epsilon_h)(\epsilon_q + p_h)}. \quad (1)$$

The system is then completely determined by firstly giving the temperature T_q of the supercooled q -phase into which the bubble is expanding. This is obtained

^{*} Here u^μ is the fluid four-velocity satisfying $u^2 = 1$. Our metric has signature $(1, -1, -1, -1)$.

from a nucleation calculation. Secondly, a microscopic calculation [23-25] gives the velocity $v_b(T_q)$ of the combustion front. This has so far been calculated for the case of $v_h - v_q \ll v_q$.

Boundary conditions often demand initial or final matter (or both) to be at rest and the single front discussed above is not sufficient. This leads one to a study of bubbles [20-21]. To understand a detonation bubble it is useful to introduce space-time rapidity,

$$y = \frac{1}{2} \ln \left(\frac{t+x}{t-x} \right) \quad (2)$$

and flow rapidity

$$\Theta = \frac{1}{2} \ln \left(\frac{1+v}{1-v} \right). \quad (3)$$

A 1-time + 1-space-dimensional detonation bubble is shown in Fig. 2, together with a plot of the flow rapidity and energy density as a function of space-time rapidity. Notice that constant space-time rapidity corresponds to $x/t \sim \text{constant}$, that is, to similarity growth. It is well known that the hydrodynamic equations admit similarity solutions. Since the front is traveling faster than sound velocity, the matter in ahead of the front is unaffected by the front until the front actually comes in contact with the matter. Behind the burning front is fast moving compressed matter, which over some region of rapidity has a constant flow velocity and energy density. The flow rapidity must be determined by solving the hydrodynamic equations. Behind this region of constant flow velocity is a similarity rarefaction wave at which the flow rapidity goes as $\Theta(y) = y - y_s$, where $y_s = \tanh c_s$ is the rapidity associated with the sound velocity c_s . The flow rapidity can vanish when the space-time rapidity is the rapidity of sound. Therefore this point moves with the sound velocity and tries to catch up with the front. It can never do so, because the front is moving supersonically. The point at which the similarity rarefaction wave begins is when $y = y_1 = y_{\text{flow}} + y_s$. In the very center of the bubble, the fluid velocity must be zero.

A deflagration bubble is shown in Fig. 3. A deflagration (slow burning) bubble propagates into the high temperature phase at a velocity less than the sound velocity of the high temperature phase. This turns out to be equivalent, in the rest frame of the burning front, to having the velocity of the fluid behind the front larger than that ahead of it. In this case, the matter in front of the bubble is compressed and accelerated to a finite velocity. In front of the burning front, the moving matter produces a shock which moves faster than the sound velocity. (This is analogous to the shock front produced by moving a piston down a pipe). Inside the burning front, the matter is at rest and at a constant density. Outside the shock front the matter is at rest and at constant density. The distance between the shock front and the burning front increases as a function of time.

To compute the properties of these detonation and deflagration bubbles, one must solve the hydrodynamic equations. In the regions between but excluding the fronts, there are acceptable solutions of the hydrodynamic equations. For the deflagration bubbles, the region excluding the front is just a fluid moving at constant velocity, which will solve the hydrodynamic equations. For the detonation bubbles, the rarefaction region has a solution which we will later explicitly compute for the electroweak phase transition.

Before explicitly solving the bubble equations, it is useful to review the properties of the solutions. For deflagrations, we know the energy density and velocity of the fluid to the right of the shock front. We know the velocity of the fluid inside the burning front. We must determine the velocity of the burning front and the shock front, the energy density inside the burning front, and the velocity and energy density of the fluid in the region between the shock front and the burning front. These are 5 unknowns. The equations for the continuity of energy and momentum flux across each front gives four equations. To solve the problem we need one more equation which is microscopic. In electroweak theory, this is the equation for the Higgs field.

For detonations, we know the velocity and energy density of the fluid to the

right of the burning front. The energy density and velocity of the fluid to the left of the burning front and the velocity of the burning front are the 3 unknowns. The continuity of energy and momentum flux are 2 equations, and again we need a microscopic equation.

The bubble solutions have been explicitly discussed in Ref. 20 for the $1 + 1$ -dimensional case and in Ref. 21 for $1 + d$, $d = 1, 2, 3$. We will now analyze these equations for the case of the electroweak phase transition.

Relevant Scales and Parameters

To proceed further, we must introduce the relevant physical quantities and identify the scales and parameters which are the most useful to the subsequent analysis. In the symmetric high temperature phase, we have

$$p_{\text{q}} = aT_{\text{q}}^4, \quad \epsilon_{\text{q}} = 3aT_{\text{q}}^4. \quad (4)$$

In the symmetry broken phase, we have

$$p_{\text{h}} = aT_{\text{h}}^4 \left[1 + \bar{L} \left(1 - \frac{T_{\text{h}}^2}{T_c^2} \right) \frac{T_c^4}{T_h^4} \right], \quad \epsilon_{\text{h}} = 3aT_{\text{h}}^4 \left[1 - \frac{\bar{L}}{3} \left(1 + \frac{T_{\text{h}}^2}{T_c^2} \right) \frac{T_c^4}{T_h^4} \right]. \quad (5)$$

Here,

$$a = g^* \frac{\pi^2}{90}$$

where $g^* \approx 107$ is the number of particle degrees of freedom. The quantity T_c is the critical temperature at which the low temperature and high temperature phase have equal free energy, that is, the phase coexistence temperature. We have introduced the dimensionless parameter \bar{L} which measures the fraction of energy released in latent heat at the phase transition

$$\bar{L} = \frac{L}{2aT_c^4} = \frac{3}{2} \frac{\epsilon_{\text{q}}(T_c) - \epsilon_{\text{h}}(T_c)}{\epsilon_{\text{q}}(T_c)}. \quad (6)$$

\bar{L} is also a measure of the efficiency of the plasma to absorb the latent heat released

at the interface; on this ground, we expect that

$$\left| \frac{T_q - T_h}{T_q} \right| \sim \bar{L}. \quad (7)$$

The important feature of the electroweak case is the intrinsic weakness of the first order phase transition due to the smallness of the parameter \bar{L} ; typically $\bar{L} \leq 0.01$. In particular, we can analytically solve for the structure of the deflagration and detonation bubbles.

A second important parameter is the relative velocity of the front with respect to the plasma, v_b , which can be written in the form

$$\gamma v_b(T_q) = \frac{V(T_q)}{\mathcal{E}} \quad (8)$$

where $V(T_q) = L(1 - T_q/T_c)$. The function \mathcal{E} is a slowly varying function of temperature, which depends on the details such as mean free paths, numbers of particles relevant at the temperature of the transition, *etc.* For our purposes, we only need to know the form of $V(T)$, and in addition, we need to know that computations of the numerical factors in the above equation, for values of T_q relevant for cosmology, give for the EW case $\gamma v_b \sim 1$ with velocities typically in the range $0.1 \leq v_b \leq 0.9$. This range reflects the dependence on the parameters of the standard model as well as the uncertainties which result in its determination [23,24]. For the QCD case smaller values, $v_b \approx 0.04$, are indicated [25]. Unfortunately, more accuracy is at present lacking for determining the burning front velocity.

There are three scales to be considered in the stability analysis of the interface to follow, and are denoted d_b , d_c and ℓ .

- d_b is a time scale characteristic of the dynamics driving the motion of the interface, defined as

$$d_b = \frac{\sigma}{V(T_q)}. \quad (9)$$

In the electroweak case, as shown in Section 4, d_b can be expressed in terms of

the thickness of the interface δ and a parameter ε ($0 < \varepsilon < 1$) proportional to the amount of supercooling in the system, as $d_b \simeq \delta/\varepsilon$.

- d_c is the scale over which the surface tension σ just balances the difference of pressure across the interface, that is,

$$d_c = \frac{\sigma}{p_q - p_h} . \quad (10)$$

Its critical role in the stability of the interface was first stressed by Landau [27]. In Section 4, it is shown that $d_c/d_b \ll 1$ for the electroweak case, an inequality that we will use later.

- ℓ is the mean free path of the particles which contribute to the heat and momentum transfer at the interface. Its effect for the electroweak transition is measured by the ratio ℓ/δ which weights the damping of the wall motion in the plasma. Because this ratio is typically less than 1, ℓ doesn't appear in the following discussions. This is not the case at the QCD scale where this ratio may be larger and can play a critical role in the stability of the interface [32]. These diffusive effects are not considered here.

Having introduced the parameters \bar{L} , v_b and the scales d_b , d_c relevant to the problem and having set their relative magnitudes, we may now proceed. We first turn to a detailed study of the kinematics of deflagrations and detonations relevant to the electroweak case. In the case of the QCD phase transition, the shapes of the bubbles are much the same as is the case for the electroweak phase transition. The essential difference is that the latent heat of the transition is larger, $\bar{L} \sim 0.5-1$, and therefore the discontinuities of energy densities are much larger. Since deflagration and detonation bubbles have been much discussed in the literature for QCD, we shall not repeat this analysis here [20].

Kinematics of Deflagrations

We first turn to the case of deflagrations. Using this parameterization of the pressure and energy density, we can now solve for the velocity of the shock front,

v_{sh} , the velocity of fluid in between the shock front and the burning front, v_{flow} , and the velocity of the deflagration (burning) front v_b denoted here by v_{def} . We define (see Fig. 3)

$$x_0 = \frac{T_0^2}{T_c^2}, \quad x_1 = \frac{T_1^2}{T_c^2}, \quad x_2 = \frac{T_2^2}{T_c^2} \quad (11)$$

with T_2 the temperature to the right hand side of the shock front and the temperature between the shock front and the burning front is T_1 . In the frame where the fluid is at rest inside the bubble, the results are

$$\begin{aligned} v_{\text{sh}} &= \sqrt{\frac{3x_1^2 + x_2^2}{3(x_1^2 + 3x_2^2)}}, \\ v_{\text{flow}} &= \sqrt{3} \frac{x_1^2 - x_2^2}{\sqrt{(3x_1^2 + x_2^2)(x_1^2 + 3x_2^2)}} \\ &= \sqrt{\frac{[x_0^2 - x_1^2 + \bar{L}(1 - x_0)][3(x_0^2 - x_1^2) - \bar{L}(1 + x_0)]}{[3x_0^2 + x_1^2 - \bar{L}(1 + x_0)][3x_1^2 + x_0^2 + \bar{L}(1 - x_0)]}}, \\ v_{\text{def}} &= \sqrt{\frac{[x_0^2 - x_1^2 + \bar{L}(1 - x_0)][3x_1^2 + x_0^2 + \bar{L}(1 - x_0)]}{[3(x_0^2 - x_1^2) - \bar{L}(1 + x_0)][3x_0^2 + x_1^2 - \bar{L}(1 + x_0)]}}. \end{aligned} \quad (12)$$

When solving the above equations, we must require that the flux associated with the entropy current

$$s^\mu = su^\mu$$

where s is the entropy density, be increased across the surfaces of discontinuity. These conditions are the same as

$$\begin{aligned} x_1 &\geq x_2 \\ (x_0 - x_1)^3 + \bar{L}(x_0 + x_1 + x_0 x_1 - \frac{3}{2}x_0^2 - \frac{3}{2}x_1^2) - \frac{1}{2}\bar{L}^2(1 - x_0) &\geq 0 \end{aligned} \quad (13)$$

When solving the above equations, we are given the parameters \bar{L} by knowing the latent heat at the phase transition, $x_2 = T_2^2/T_c^2$ by knowing the amount of

supercooling from the nucleation calculation, and v_{def} by solving the microscopic equations for the burning front velocity.

For the weak deflagrations typical of the electroweak phase transition, we can solve the equations explicitly. We have $T_2 < T_c$ and assume that $T_0 - T_1 \approx T_2 - T_1 \ll T_c$. The regions where there are allowed solutions for the above equations are then shown in Fig. 4. The linear boundaries of the regions, given in the figure, correspond to $v_h = v_q = 0$, $v_h = v_q = 1$, $\Delta s_\perp = 0$ [22]. The temperature inside the bubble is

$$\frac{T_0 - T_2}{T_2} = \frac{\bar{L}}{6} \frac{\sqrt{3}v_{\text{def}}}{1 + \sqrt{3}v_{\text{def}}}. \quad (14)$$

The temperature in the region between the shock front and the deflagration front is

$$\frac{T_1 - T_2}{T_2} = \frac{\bar{L}}{6} \frac{\sqrt{3}v_{\text{def}}}{1 - 3v_{\text{def}}^2}. \quad (15)$$

Notice that $T_1 \geq T_0 \geq T_2$ and that (Fig. 4) $T_0 < T_c$. The flow velocity of the matter between the deflagration front and the shock front is

$$v_{\text{flow}} = \frac{3v_{\text{def}}^2}{1 - 3v_{\text{def}}^2}. \quad (16)$$

There is a singularity in these equations when $v_{\text{def}}^2 \rightarrow 1/3$, which is an artifact of our approximate solution. When the burning velocity is very close to that of the sound velocity in the supercooled phase, then the temperatures are not so close to one another.

Since there is no reason for the burning velocity to be close to the sound velocity, the solution above is sufficient for most purposes. For the weak first order electroweak phase transition, the temperature is only slightly changed in the flow region and the interior of the bubble wall. The velocity of the fluid is of order v_{def}^2 which becomes of order 1 only for deflagration velocities close to that of the sound velocity.

Kinematics of Detonations

In the case of detonation bubbles, we have one surface of discontinuity corresponding to the burning front. Behind the burning front, we must have a similarity rarefaction solution of the hydrodynamic equations. We assume that in the region of the similarity rarefaction wave, the equation of state of the fluid is close to that of an ideal gas. In this case, we can solve the hydrodynamic equations to find

$$\Theta = y - y_s$$

and

$$\epsilon = \epsilon(y_s) e^{4(y-y_s)/\sqrt{3}}. \quad (17)$$

We can now solve for the velocities and energy densities in the various regions subject to the constraint of positive entropy generation. In the region of small temperature changes we find that

$$\frac{\epsilon_1 - \epsilon_2}{\epsilon_2} = \frac{2}{3} \frac{\bar{L}}{3v_{\text{det}}^2 - 1} \quad (18)$$

and

$$v_{\text{flow}} = \frac{\bar{L}}{2} \frac{v_{\text{det}}}{3v_{\text{det}}^2 - 1}. \quad (19)$$

The energy density far in the interior of the bubble is given by

$$\frac{\epsilon_0 - \epsilon_2}{\epsilon_2} = -\frac{2}{3} \frac{(1 - \sqrt{3})\bar{L}}{3v_{\text{det}}^2 - 1}. \quad (20)$$

We therefore see that in the energy density in the interior of the bubble is decreased relative to that in the outer region. The matter density in the flow region is compressed. Again the changes are small unless the burning front velocity is close to that of the sound velocity. In this case our analysis must be modified.

3. Stability of Relativistic Planar Combustion Fronts

In this section we study the stability of planar relativistic combustion fronts. The problem has been studied in the non-relativistic case by Landau [27] and by Link [26] for non-relativistic velocities but for a relativistic equation of state. The result is basically as follows. Small perturbations of deflagration fronts are stabilized by the interface tension σ while large ones grow exponentially with an initial growth time

$$\Omega^{-1} \simeq \frac{4}{L} \frac{1}{v_b} \frac{\lambda^2}{\lambda - \lambda_c} \quad (21)$$

where λ_c is the critical length scale (10) introduced in the previous section

$$\lambda_c = d_c . \quad (22)$$

We would like to make two modifications to these earlier works. First, in order to treat properly the critical role played by the speed of sound $c_s \simeq 1/\sqrt{3}$, the hydrodynamic equations will be written in a completely relativistic form. We can thus study the stability for fast deflagrations, $v_h \rightarrow c_s$ and also the stability of detonations, $v_q > v_h, v_q \geq c_s$. Secondly, we have now available several microscopic estimates of the interface velocity v_b , at least for the case $v_h - v_q \ll v_h$ [23-25]. In particular, this velocity will depend on the temperature $T_q \approx T_h < T_c$. We shall see that if this dependence is sufficiently strong – as seems to be the case for the electroweak theory – the conclusions on the stability are completely changed: the dependence of v_b on T_q actually stabilizes large scale perturbations of a deflagration burning front.

The stability analysis proceeds as follows. First the leading hydrodynamic solution, a sharp planar combustion front separating a region characterized by T_q, v_q from a region characterized by T_h, v_h is described [20]. Secondly, the relativistic hydrodynamic equations are linearized separately in the two regions around a leading $T = \text{constant}, v = \text{constant}$ solution (see also Ref. [28]) and the linear equations

so obtained are solved for the Fourier components of the perturbations of T and v . The subtle aspect of the analysis is then the joining of the solutions in the two regions across a perturbed interface. The outcome of the stability analysis depends on whether or not the connection equations have solutions with $\Omega = -i\omega > 0$; such solutions grow like $\exp(\Omega t)$ and constitute an instability.

Deflagrations and Detonations

Here we review the results of Section 2 and formulate them in a form more suitable to our purpose. The leading solution is defined as follows. In the rest frame of the combustion front (assumed to be in the x, y -plane), the velocities are parallel to the z -axis and the $q(h)$ -phase lies in the region $z < 0$ ($z > 0$) (see Fig. 1). We assume that the chemical potential $\mu = 0$ and that the equations of state $p = p(T)$ are known. The configuration is thus entirely determined by the four quantities T_q , T_h , v_q , v_h . These are constrained by the continuity of energy and momentum fluxes:

$$\begin{aligned} w_q \gamma_q^2 v_q &= w_h \gamma_h^2 v_h \equiv F_\epsilon \\ w_q \gamma_q^2 v_q^2 + p_q &= w_h \gamma_h^2 v_h^2 + p_h \quad \text{or} \quad F_\epsilon(v_h - v_q) = p_q - p_h \end{aligned} \tag{23}$$

where $w = p + \epsilon$ is the enthalpy of the fluid, and of entropy increase

$$s_h \gamma_h v_h \geq s_q \gamma_q v_q. \tag{24}$$

Thus two of the four quantities remain unspecified by these general relations.

Information on the further two required relations is obtained from nucleation calculations and from microscopic calculations of the wall velocity. The nucleation calculations give some temperature $T_q < T_c$ of the q -phase, into which the bubbles of the h -phase have to expand. However, as described at length in Section 2, boundary condition effects (matter at rest before and after the transition) may require the q -matter in front of the interface to be shocked, *i.e.*, have a temperature higher than the nucleation temperature. Similarly, a microscopic calculation of v_b

gives v_h if boundary conditions demand the h -matter behind the front to be at rest or v_q if the q -matter in front of the front is at rest. This distinction is not important if $v_h - v_q \ll v_h$. This is the case for the EW transition, as we note from the constancy of F_ϵ [Eq. (23)] and the definition of \bar{L} [Eq. (6)], that

$$\frac{v_h - v_q}{v_q} \simeq \frac{w_q(T_c) - w_h(T_c)}{w_h(T_c)} = \frac{\bar{L}}{2} \leq 0.01. \quad (25)$$

The reason why this velocity difference is so small in the electroweak phase transition is because the transition is rather weakly first order, most of the inertia of the matter is carried by light mass degrees of freedom which are not much affected by the transition and even the W, Z and Higgs bosons gain a mass which is small compared to a typical kinetic energy $E \sim 3T$.

Linearized Hydrodynamic Equations

We shall now consider either the q - or the h - region and linearize the hydrodynamic equations $\partial_\mu \Theta^{\mu\nu} = 0$, $\Theta^{\mu\nu} = w u^\mu u^\nu - p g^{\mu\nu}$, $u^\mu = (\gamma, \gamma \mathbf{v})$, around a solution $T = \text{constant}$, $\mathbf{v} = (0, 0, v) = \text{constant}$. We shall use as variables $\delta p = \delta w / (1 + 1/c_s^2)$, δv and the transverse 4-velocity variation u^\perp . We assume that the sound velocity is the same in the q - and h - phases. Instead of v it is often convenient to use the flow rapidity θ related to it by $v = \tanh \theta$, $\delta \theta = \gamma^2 \delta v$. Thus we write

$$\begin{aligned} p &= p_0 + \delta p \\ u^\mu &= u_0^\mu + \delta u^\mu = (\cosh \theta, 0, 0, \sinh \theta) + (\sinh \theta \ \delta \theta, 0, u^\perp, \cosh \theta \ \delta \theta) \end{aligned} \quad (26)$$

The components of the zeroth- and first-order variations of the energy momentum

tensor are then

$$\begin{aligned}
\Theta^{00} &= w \cosh^2 \theta - p & \delta\Theta^{00} &= [(1 + c_s^{-2}) \cosh^2 \theta - 1] \delta p + w \sinh 2\theta \delta\theta \\
\Theta^{0z} &= \frac{1}{2} w \sinh 2\theta & \delta\Theta^{0z} &= (1 + c_s^{-2}) \frac{1}{2} \sinh 2\theta \delta p + w \cosh 2\theta \delta\theta \\
\Theta^{0\perp} &= 0 & \delta\Theta^{0\perp} &= w \cosh \theta u^\perp \\
\Theta^{zz} &= w \sinh^2 \theta + p & \delta\Theta^{zz} &= [(1 + c_s^{-2}) \sinh^2 \theta + 1] \delta p + w \sinh 2\theta \delta\theta \\
\Theta^{z\perp} &= 0 & \delta\Theta^{z\perp} &= w \sinh \theta u^\perp \\
\Theta^{\perp\perp} &= p & \delta\Theta^{\perp\perp} &= \delta p
\end{aligned} \tag{27}$$

The subscript 0 is omitted from w_0 and v_0 whenever no confusion arises.

The linearized equations $\partial_\mu \delta\Theta^{\mu\nu} = 0$ can then be written in a particularly symmetric form by using light cone derivatives $\partial_\pm = e^{\mp\theta}(\partial_0 \pm \partial_z)$:

$$\begin{aligned}
\frac{1}{2}(c_s^{-2} + 1)\partial_+\delta p + \frac{1}{2}(c_s^{-2} - 1)\partial_-\delta p + w\partial_+\delta\theta + w\partial_\perp u^\perp &= 0, \\
\frac{1}{2}(c_s^{-2} - 1)\partial_+\delta p + \frac{1}{2}(c_s^{-2} + 1)\partial_-\delta p - w\partial_-\delta\theta + w\partial_\perp u^\perp &= 0, \\
\partial_\perp \delta p + \frac{1}{2}w(\partial_+ + \partial_-)u^\perp &= 0,
\end{aligned} \tag{28}$$

Similarly, the first order variation of the entropy conservation equation $\partial_\mu \delta s^\mu = 0$ (valid in the bulk fluid, far from the wall) becomes

$$\frac{1}{2}c_s^{-2}(\partial_+ + \partial_-)\delta p + \frac{1}{2}w(\partial_+ - \partial_-)\delta\theta + w\partial_\perp u^\perp = 0. \tag{29}$$

Fourier Solution of the Linearized Hydrodynamic Equations

We shall now search for solutions of Eqs. (28) of the form

$$\delta\theta = Ae^{-ik\cdot x}, \quad u^\perp = Be^{-ik\cdot x}, \quad \delta p = Ce^{-ik\cdot x}. \tag{30}$$

Since we are interested in solutions behaving as $e^{\Omega t}$ but which do not blow up at large distances, it is convenient to introduce $\Omega = -i\omega$ and $q = ik_z$ and write the

exponent in the form

$$-ik \cdot x = \Omega t + qz + ikx^\perp. \quad (31)$$

The insertion of Eq. (30) into Eq. (28) gives a linear homogeneous system of equations for the Fourier components A, B and C . In general there is a dispersion relation

$$\frac{1}{c_s^2}(\Omega + vq)^2 - (q + v\Omega)^2 + \frac{1}{\gamma^2}k^2 = 0 \quad (32)$$

relating the components of the wavevector, and one can express δp and u^\perp in terms of $\delta\theta$. We find two types of solutions:

$$\delta p = -w \frac{\Omega + vq}{v\Omega + q} \delta\theta, \quad u^\perp = \frac{ik}{v\Omega + q} \frac{1}{\gamma} \delta\theta. \quad (33)$$

and

$$\delta p = 0, \quad ik u^\perp = \frac{-q}{\gamma} \delta\theta. \quad (34)$$

The latter is a special solution which describes an incompressible velocity perturbation ($\nabla \cdot \delta\mathbf{v} = 0$) moving with the fluid, *i.e.*, it is only a function of $z - vt, x^\perp$; it is characterized by

$$\Omega = -vq. \quad (35)$$

The dispersion relation, Eq. (32), deserves further attention; on the (Ω, q) plane, it appears as the hyperbolae

$$q_\pm = \frac{v(1 - c_s^2)\Omega \pm c_s(1 - v^2)\sqrt{\Omega^2 + (c_s^2 - v^2)\gamma^2 k^2}}{(c_s^2 - v^2)} \quad (36)$$

with the asymptotes

$$\Omega = \frac{c_s - v}{1 - vc_s} q, \quad \Omega = -\frac{c_s + v}{1 + c_s v} q. \quad (37)$$

It is plotted in Figs. 5. From the asymptotes one sees that for $v < c_s$ both branches of the curve extend over all values of Ω . However, for $v > c_s$, one finds

$q > 0$ (actually $q \geq \sqrt{1 - v^2 c_s^2} \gamma k$) only for $\Omega < 0$ and vice versa. More generally, it is a simple exercise to show that the dispersion relation (32) has no solution with $v \geq c_s \geq 0$, $\text{Re } q > 0$ and $\text{Re } \Omega > 0$. This fact is of great importance for it establishes at once the stability of a detonation front. Indeed, in Section 2, we have learned that a detonation front is characterized by $v_q > c_s, v_h$. On the other hand, the perturbation behaves like $\exp(zq_q)$; as the q -phase lies in the region $z \leq 0$,^{*} this requires $\text{Re } q_q \geq 0$. Hence, there is no possible unstable mode ($\text{Re } \Omega > 0$) in a detonation front. In the remainder of our discussions, we will assume that we are dealing with deflagration burning fronts only.

Connecting the Solutions

We now return to the two-phase situation depicted in the beginning of this section and study how its small oscillations behave if the interface is perturbed from $z = 0$ to

$$z = \zeta(t, x^\perp) = De^{\Omega t + ikx^\perp}, \quad (38)$$

where the amplitude D of the perturbation satisfies

$$\delta \ll D \ll 1/k, 1/\Omega. \quad (39)$$

The condition that $D \gg \delta$ is just the requirement that we are looking for macroscopic fluctuations in the shape of the wall, that is their characteristic size scale is much larger than the thickness of the wall δ . The condition that $D \ll 1/k, 1/\Omega$ is the requirement that we are looking at small fluctuations. The solutions in the q -phase ($z < \zeta$) and in the h -phase ($z > \zeta$) can be immediately written down. Omitting a common factor of $e^{\Omega t + ikx^\perp}$ the solution in the q -phase is

$$\begin{aligned} \delta\theta_q &= A, \\ \delta p_q &= -w_q \frac{\Omega + v_q q_q}{v_q \Omega + q_q} A, \\ u_q^\perp &= \frac{ik}{v_q \Omega + q_q} \frac{1}{\gamma_q} A, \end{aligned} \quad (40)$$

* Physically imposed after the choice $v_q \geq 0$.

where $q_{\mathbf{q}} > 0$ (to make the perturbation vanish as $z \rightarrow -\infty$). This requirement and the fact that we are searching for $\Omega > 0$ formally imply that one cannot include the special solution (34) with the dispersion relation $\Omega = -vq$ in this region, as already emphasized by Landau [27]. However, in the \mathbf{h} -region we must have $q_{\mathbf{h}} < 0$ and the special solution can (and must) be included:

$$\begin{aligned}\delta\theta_{\mathbf{h}} &= B + C, \\ \delta p_{\mathbf{h}} &= -w_{\mathbf{h}} \frac{\Omega + v_{\mathbf{h}} q_{\mathbf{h}}}{v_{\mathbf{h}} \Omega + q_{\mathbf{h}}} B, \\ u_{\mathbf{h}}^{\perp} &= ik \left[\frac{1}{v_{\mathbf{h}} \Omega + q_{\mathbf{h}}} \frac{1}{\gamma_{\mathbf{h}}} B - \frac{\Omega}{k^2 v_{\mathbf{h}} \gamma_{\mathbf{h}}} C \right].\end{aligned}\tag{41}$$

To see the physics of the special solution, one may compute

$$(\nabla \times \delta \mathbf{v}_{\mathbf{h}})^i = \epsilon_{i\perp z} \frac{k}{\gamma_{\mathbf{h}}^2} \left\{ \frac{v_{\mathbf{h}} \Omega}{v_{\mathbf{h}} \Omega + q_{\mathbf{h}}} B + \left[1 - \left(\frac{\Omega}{kv_{\mathbf{h}}} \right)^2 \right] C \right\};$$

in the \mathbf{q} -phase no C term appears. As a consequence, in the non-relativistic limit $v \ll 1$ this vanishes in the \mathbf{q} -phase and is nonzero in the \mathbf{h} -phase: linear perturbations of the interface generate vortices which, through the special solution, propagate in the \mathbf{h} -phase.

We thus have four unknowns, A , B , C and D and need four equations to determine them (or their ratios). Three of the four conditions are obtained by expressing conservation of energy-momentum across the interface $\partial_{\mu} \Theta^{\mu\nu} = 0$ for $\nu = \perp, 0, z$. Here, $\Theta^{\mu\nu}$ is the total stress-energy tensor of the system including the interface

$$\Theta^{\mu\nu} = \Theta_{\mathbf{q}}^{\mu\nu} \theta \left[-z + \zeta(t, x^{\perp}) \right] + \Theta_{\mathbf{h}}^{\mu\nu} \theta \left[z - \zeta(t, x^{\perp}) \right] + \Theta_K^{\mu\nu} \left\{ \phi_K \left[z - \zeta(t, x^{\perp}) \right] \right\}.\tag{42}$$

The two first terms are straightforward, with $\Theta_{\mathbf{q}}^{\mu\nu}$ and $\Theta_{\mathbf{h}}^{\mu\nu}$ constant. The third term describes the stress-energy arising from distorting the kink solution of the

interface, assumed here to be infinitely thin. We have

$$\Theta_K^{\mu\nu} = \partial^\mu \phi \partial^\nu \phi - g^{\mu\nu} \left[\frac{1}{2} \partial_\lambda \phi \partial^\lambda \phi - V(\phi) \right],$$

with the kink solution satisfying

$$\phi''_K(z) = V'(\phi_K), \quad \frac{1}{2} [\phi'_K(z)]^2 = V(\phi_K). \quad (43)$$

Calculating to first order in ζ one finds that

$$\Theta_K^{\mu\nu} = \begin{pmatrix} \sigma(z) - \zeta \sigma'(z) & 0 & 0 & \sigma(z) \partial_0 \zeta \\ 0 & -\sigma(z) + \zeta \sigma'(z) & 0 & -\sigma(z) \partial_x \zeta \\ 0 & 0 & -\sigma(z) + \zeta \sigma'(z) & -\sigma(z) \partial_y \zeta \\ \sigma(z) \partial_0 \zeta & -\sigma(z) \partial_x \zeta & -\sigma(z) \partial_y \zeta & 0 \end{pmatrix}, \quad (44)$$

where the notation (for the surface tension)

$$\sigma(z) = [\phi'_K(z)]^2 \approx \sigma \delta(z - \zeta), \quad \sigma = \int dz \sigma(z), \quad (45)$$

has been introduced.

If we now compute $\partial_\mu \Theta^{\mu\nu}$ from Eq. (42), the result is proportional to $\delta(z - \zeta)$. For the two first terms this arises as the derivative of the θ -function. For the kink term, Eq. (44) gives $\partial_\mu \Theta_K^{\mu\nu} = \sigma(z) \partial^2 \zeta \delta^{\nu z}$, which again, within the approximation (45), is proportional to $\delta(z - \zeta)$. A quantity proportional to a δ function can only vanish if the coefficient of the δ function vanishes. We thus obtain, at the wall:

$$\Theta_{\mathbf{q}}^{z\nu} = \Theta_{\mathbf{h}}^{z\nu} \quad (46)$$

$$[\delta \Theta_{\mathbf{q}}^{z\nu} - \Theta_{\mathbf{q}}^{0\nu} \partial_0 \zeta - \Theta_{\mathbf{q}}^{\perp\nu} \partial_\perp \zeta] - [\mathbf{q} \rightarrow \mathbf{h}] - \sigma(\partial_0^2 - \partial_\perp^2) \zeta \delta^{z\nu} = 0. \quad (47)$$

The first equations reproduce the leading conservation conditions (23).^{*} The others give us three linear relations between the coefficients A , B , C , and D .

* In general, there is a term on the RHS of Eq. (46) involving the extrinsic curvature of the wall.

A fourth equation can be obtained by expressing conservation of entropy across the wall,

$$\gamma_q v_q s_q = \gamma_h v_h s_h + \int_{wall} J_{source}, \quad (48)$$

where the last term on the right-hand side is a measure of the flux of entropy gained by the plasma as it crosses the wall. From the work of Refs. [23–25], it has been established that entropy generation reflects directly the existence of a velocity dependent force which damps the wall motion to a terminal velocity. This velocity was discussed in the second section,

$$(\gamma v)_b = \frac{V(T_q)}{\mathcal{E}}. \quad (49)$$

This equation of motion has to be modified to include the effect of the curvature of the interface as well as of its acceleration, namely,

$$\sigma (\partial_0^2 - \partial_\perp^2) \zeta = -V(T_q) + (\gamma v)_b \mathcal{E}. \quad (50)$$

Equation (49) yields a unique value for the entropy source in (48) and, consequently, can be alternatively used to generate the needed fourth relation. After linearizing Eq. (50), we obtain

$$v_q d_b (\partial_0^2 - \partial_\perp^2) \zeta = (\delta \theta_q - \gamma_q^2 \partial_0 \zeta) - \eta \delta \theta_q \quad (51)$$

where $d_b = \sigma/V(T_q)$, a scale we have already introduced in Eq. (9), and where one has defined

$$\begin{aligned} \eta &= - \left(-T_c \frac{dv_b}{dT_q} \right) \frac{1}{w_q} \frac{\delta p_q}{\delta \theta_q} \\ &= \left(-T_c \frac{dv_b}{dT_q} \right) \frac{\Omega + v_q q_q}{v_q \Omega + q_q} \\ &\simeq \left(-T_c \frac{dv_b}{dT_q} \right) v_b. \end{aligned} \quad (52)$$

The latter approximation will be justified later.

Equations (47) and (51) form a complete set of homogeneous linear equations

$$\frac{1}{\gamma_q} u_q^\perp + v_q \partial_\perp \zeta = \frac{1}{\gamma_h} u_h^\perp + v_h \partial_\perp \zeta. \quad (53)$$

$$\begin{aligned} (1 + c_s^{-2}) \gamma_q^2 v_q \delta p_q + w_q \gamma_q^2 (1 + v_q^2) (\delta \theta_q - \partial_0 \zeta) \\ = (1 + c_s^{-2}) \gamma_h^2 v_h \delta p_h + w_h \gamma_h^2 (1 + v_h^2) (\delta \theta_h - \partial_0 \zeta). \end{aligned} \quad (54)$$

$$\begin{aligned} \left[(1 + c_s^{-2}) \gamma_q^2 v_q^2 + 1 \right] \delta p_q + 2 w_q \gamma_q^2 v_q \delta \theta_q - \sigma (\partial_0^2 - \partial_\perp^2) \zeta \\ = \left[(1 + c_s^{-2}) \gamma_h^2 v_h^2 + 1 \right] \delta p_h + 2 w_h \gamma_h^2 v_h \delta \theta_h. \end{aligned} \quad (55)$$

$$\gamma_q^2 \partial_0 \zeta + v_q d_b (\partial_0^2 - \partial_\perp^2) \zeta = (1 - \eta) \delta \theta_q. \quad (56)$$

Eq. (53) relates the changes of transverse velocity while Eqs. (54) and (55) describe the conservation of the flow of energy and momentum respectively. If η were zero, Eq. (56) tells us that the velocity v_b of the interface relative to the q -phase is only perturbed by surface tension effects; this is akin to the boundary condition initially used by Landau.^{*} However, due to the potential dependence of the interface velocity on the temperature, this is no longer true and the η term is needed. Furthermore, Eq. (56) provides a direct physical interpretation of the stability of a deflagration that we will uncover in the next section. We now proceed to the resolution of this system of equations.

Solution for Small Velocities

The case of general velocities results in rather lengthy equations and we shall first discuss the solution for small velocities. In this case, the equations are much simpler and their interpretation is more transparent. This case is defined by

* In his analysis, Landau further ignored the effects of the surface tension. This is reasonable for most of the applications.

$v_{\mathbf{q}}, v_{\mathbf{h}} \ll c_s$ for which, the integrability condition (32) simply implies

$$q_{\mathbf{q}} \simeq k, \quad q_{\mathbf{h}} \simeq -k, \quad |\omega| \sim v k. \quad (57)$$

As a result the solutions in the \mathbf{q} - and \mathbf{h} -phases simplify to

$$\begin{aligned} \delta v_{\mathbf{q}} &= A & \delta v_{\mathbf{h}} &= B + C \\ \delta p_{\mathbf{q}} &= -w_{\mathbf{q}} \left(\frac{\Omega}{k} + v_{\mathbf{q}} \right) A & \delta p_{\mathbf{h}} &= w_{\mathbf{h}} \left(\frac{\Omega}{k} - v_{\mathbf{h}} \right) B \\ u_{\mathbf{q}}^{\perp} &= iA, & u_{\mathbf{h}}^{\perp} &= -i \left(B + \frac{\Omega}{v_{\mathbf{h}} k} C \right). \end{aligned} \quad (58)$$

After inserting these expressions into Eqs. (53)–(56) and using (23) and (25) as well as the definitions of d_c , we obtain

$$\begin{pmatrix} 1 & 1 & \frac{\Omega}{kv_{\mathbf{h}}} & -v_{\mathbf{q}} \frac{\bar{L}}{2} \\ v_{\mathbf{h}} & -v_{\mathbf{q}} & -v_{\mathbf{q}} & -v_{\mathbf{q}} \frac{\bar{L}}{2} \frac{\Omega}{k} \\ \left(\frac{\Omega}{kv_{\mathbf{q}}} - 1 \right) & \left(\frac{\Omega}{kv_{\mathbf{h}}} + 1 \right) & 2 & v_{\mathbf{q}} \frac{\bar{L}}{2} d_c k \\ -(1 - \eta) & 0 & 0 & \left(\frac{\Omega}{k} + v_{\mathbf{q}} d_b k \right) \end{pmatrix} \begin{pmatrix} A \\ B \\ C \\ D \end{pmatrix} = 0. \quad (59)$$

A non trivial solution exists if and only if the determinant of the matrix in Eq. (59) vanishes, that is,

$$\Omega = kv_{\mathbf{h}} \quad (60)$$

or

$$v_{\mathbf{q}}^2 (1 - \eta) \frac{\bar{L}}{2} \left(\frac{k}{k_c} - 1 \right) + 2v_{\mathbf{q}} \left[1 + \eta \frac{\bar{L}}{2} + d_b k \right] \frac{\Omega}{k} + \left[1 + \frac{v_{\mathbf{q}}}{v_{\mathbf{h}}} + \frac{v_{\mathbf{q}}}{v_{\mathbf{h}}} \eta \frac{\bar{L}}{2} \right] \left(\frac{\Omega}{k} \right)^2 = 0. \quad (61)$$

with

$$\lambda_c = k_c^{-1} = d_c \left(1 + \frac{2}{1 - \eta} \frac{2}{\bar{L}} \frac{d_b}{d_c} \right) \quad (62)$$

defined as the critical wavelength. The first solution (60) is spurious and has no physical significance. It leads to $A = D = B + C = 0$ and from Eq. (58) the

entire solution vanishes. In general, it lies at $\Omega = \gamma_h v_h k$, and the solution vanishes likewise. The smallness of v_q insures that the term quadratic in Ω is small and the solution is

$$\frac{\Omega}{k} \simeq \frac{\bar{L}}{4} \frac{v_b(1-\eta)(1-k/k_c)}{1+\eta \bar{L}/2 + d_b k}. \quad (63)$$

For our purpose, Eq. (63) adequately generalizes the original Landau formula (21). Accordingly, the condition of stability becomes

$$(1-\eta)(\lambda - \lambda_c) < 0. \quad (64)$$

If $\eta < 1$ the system is unstable for perturbations of scale λ larger than λ_c . This is the case if the wall velocity v_q depends sufficiently weakly on T_q . However, if this dependence is strong enough to make $\eta > 1$, *large scale perturbations become stable*.

We can now comment on two numerical approximations made earlier. Firstly, it is obvious from Eq. (63) that Ω is of the order of $\bar{L}v_q k$ so that indeed the relevant range of Ω is $\leq v k$. Secondly, including the Ω dependence of η in Eq. (61) would amount to $v_q \rightarrow v_q + \Omega/k$. However, the additional (positive) term would not contribute to the Ω -independent terms and thus is irrelevant for the stability consideration.

We now turn to the interpretation of the results (62)–(64). First, we note that the critical wavelength λ_c [Eq. (62)] receives a correction of order \bar{L}^{-1} in respect to Landau's value d_c [Eq. (22)]; this term originates from the RHS of Eq. (50). In a typical macroscopic situation, the latent heat released is a significant fraction of the total energy available ($\bar{L} \gg 1$) and this correction is negligible. However, in the extremely weak phenomena considered here ($\bar{L} < 1$), this correction is large and actually controls the value of λ_c .

- If $\eta \ll 1$, $\lambda_c \simeq (4/\bar{L}) d_b$ and is significantly larger than d_c because of the smallness of \bar{L} and of the ratio d_c/d_b .

- If $\eta \gg 1$, $\lambda_c \simeq -(1/\eta) (4/\bar{L}) d_b$ and is driven negative; in which case, according to Eq. (64), *perturbations at all scales are stable*.

The physics of this stability restoration depending on the size of η is as follows. For the sake of simplicity, let us ignore (with Landau) the RHS of Eq. (51) which doesn't play any role in the argument. In the limit $\eta \rightarrow 0$, Eq. (51) reproduces Landau's boundary condition. In such a case, the velocity of the perturbation $\partial_0 \zeta$ follows the variations in velocity of the fluid. This drives perturbations larger and larger unless the surface energy $\partial_\perp^2 \zeta \sim \zeta/\lambda^2$ is significant enough to prevent their growth; this occurs for λ sufficiently small. In the present case, the interface velocity [Eq. (49)] is proportional to $V(T_q)$, an extremely sensitive function of the temperature of the q -phase; this sensitivity is measured by η . The growing perturbation triggers a local variation in temperature^{*} which affects, in turn, the velocity independent pressure $V(T_q)$ acting on the interface. This increase or decrease in pressure acts as a restoring force which opposes the growth of the perturbation. When this force is large enough to dominate the others ($\eta > 1$), the perturbation collapses. This mechanism operates only if the characteristic growth time of the perturbation is larger than the time scale which characterizes the wall dynamics, that is, only if $\Omega d_b < 1$. This condition is amply satisfied in the cases of interests.[†]

At this point we may also compare with the 4th equation used by Link [26] which in the present notation is

$$\Omega A = A + \frac{3v_q}{4v_h} \alpha \left[\left(\frac{\Omega}{k} + v_q \right) A + \left(\frac{\Omega}{k} - v_h \right) B \right], \quad (65)$$

where $0 \leq \alpha \leq 1$ is a phenomenological parameter used to describe the magnitude of F_ϵ in terms of $T_q^4 - T_h^4$. It is evident that in this case the additional term is only a small correction to A and will not modify the conclusions about stability. Our calculation, on the other hand, is based on an explicit calculation of $F_\epsilon =$

* Positive or negative depending on its direction of growth.

† As $\Omega \ll k$ and k is restricted by Eq. (39).

$w_{\mathbf{q}}\gamma_{\mathbf{q}}^2 v_{\mathbf{q}}(T_{\mathbf{q}})$ and indicates that this dependence may be strong enough to actually make large scales stable.

Solution for Arbitrary Velocities

As mentioned earlier, the speed of sound c_s plays a critical role in the stability of a moving front. In order to extend the previous conclusions to velocities ranging up to c_s , one has to generalize the analysis of the previous section. It is convenient to introduce the dimensionless quantities

$$\widehat{\Omega} = \frac{\Omega}{\gamma_{\mathbf{h}} v_{\mathbf{h}} k} \quad (66)$$

$$\begin{aligned} \Delta_{\mathbf{h}} &= \sqrt{1 - \frac{v_{\mathbf{h}}^2}{c_s^2}}, & S_{\mathbf{h}}(\widehat{\Omega}) &= \sqrt{\widehat{\Omega}^2 \frac{v_{\mathbf{h}}^2}{c_s^2} + \Delta_{\mathbf{h}}^2} \\ \Delta_{\mathbf{q}} &= \sqrt{1 - \frac{v_{\mathbf{q}}^2}{c_s^2}}, & S_{\mathbf{q}}(\widehat{\Omega}) &= \sqrt{\widehat{\Omega}^2 \frac{v_{\mathbf{h}}^2}{c_s^2} + \Delta_{\mathbf{q}}^2 \frac{\gamma_{\mathbf{q}}^2}{\gamma_{\mathbf{h}}^2}}. \end{aligned} \quad (67)$$

The calculation of the determinant proceeds exactly as before and we will only quote the results here. Neglecting once again the spurious solution $\widehat{\Omega} = 1$, we may write the determinantal equation in the form:

$$\widehat{\Omega} \mathcal{D}(\widehat{\Omega}) = \mathcal{N}(\widehat{\Omega}). \quad (68)$$

\mathcal{N} and \mathcal{D} are two lengthy polynomials in $\widehat{\Omega}$, $S_{\mathbf{q}}$ and $S_{\mathbf{h}}$. \mathcal{D} is a positive quantity unless k/k_c is excessively large, while \mathcal{N} contains the critical information on the stability behavior we have uncovered in the small velocity limit. A closer inspection of Eq. (68) reveals that the absolute value of $\widehat{\Omega}$ ($= |\mathcal{N}/\mathcal{D}|$) is bounded from above and is never much larger than one. Consequently, we can attempt to solve (68) iteratively in the following manner

$$\widehat{\Omega}_0 = \frac{\mathcal{N}(0)}{\mathcal{D}(0)}, \quad \widehat{\Omega}_1 = \frac{\mathcal{N}(\widehat{\Omega}_0)}{\mathcal{D}(\widehat{\Omega}_0)}, \quad \text{etc.} \quad (69)$$

This iteration converges very rapidly. A comparison of the lowest order of this approximation with a numerical analysis shows an agreement better than one percent

over the whole range of velocities. We then obtain

$$\frac{\Omega}{k} \simeq \gamma_h v_h \frac{\mathcal{N}(0)}{\mathcal{D}(0)} \quad (70)$$

with

$$\begin{aligned} \mathcal{N}(0) &= (1 - \eta) \frac{\bar{L}}{2} \gamma_q v_q \Delta_q \left(1 - \frac{k}{k_c} \right) \Delta_h \\ \mathcal{D}(0) &\simeq \gamma_h v_h \left(\Delta_h + \Delta_q \frac{v_h}{v_q} \right) \gamma_q^2 + \gamma_q v_q d_b k \left(\Delta_h + \frac{v_h}{v_q} \Delta_q \right) \\ &+ \eta \frac{\bar{L}}{2} \left\{ \Delta_q \gamma_h v_h + \Delta_h \gamma_q v_q [\Delta_q + (2 + \Delta_q^2) \gamma_q v_q \gamma_h v_h] \right. \\ &\left. - \gamma_q v_q d_b k \left[\Delta_q \gamma_h^2 v_h^2 \left(1 + \frac{3}{1 + \Delta_h} \right) + v_q v_h \gamma_q^2 \gamma_h^2 (2 + \Delta_q^2) (1 + v_h^2) \right] \right\} \end{aligned} \quad (71)$$

and

$$\lambda_c = k_c^{-1} = d_c \frac{\gamma_h (1 + v_h^2)}{\Delta_h} + \frac{2}{1 - \eta} \frac{1}{\bar{L}} d_b \left(\frac{v_h}{\Delta_h} + \frac{v_q}{\Delta_q} \right) \frac{1}{v_q \gamma_q} \quad (72)$$

Solution (70), along with (72), suitably generalizes the corresponding expressions (63) and (62) for velocities ranging up to c_s . As a first check, the reader may verify that, as v_q and v_h approach zero, S_q , S_h , Δ_h and Δ_q all approach unity and Eqs. (70) and (72) reproduce the familiar small velocity results. Furthermore, the condition for stability of a disturbance reads

$$\mathcal{N}(\hat{\Omega} = 0) \leq 0 \quad (73)$$

and it is clear that all the conclusions reached previously hold. In particular, $\eta > 1$ stabilizes the long wavelength modes.

As $v_h \rightarrow c_s$, the quantity $\Delta_h \rightarrow 0$ and expression (72) indicates that $\lambda_c \rightarrow \infty$ in this limit; in such a case, our solution (70) is no longer appropriate.* However, one

* Only for $v_h/c_s > 0.99$.

may show, using the full secular equation (68), that, in this limit, the determinant possesses no positive roots for any value of k . This result matches nicely with the stability of detonations.

4. Applications to the EW and QCD Phase Transitions

In this section we apply the results of the previous sections to the evolution of an expanding bubble of true vacuum produced at the electroweak phase transition. The characteristics of the electroweak phase transition are entirely encoded in the finite temperature effective potential for the Higgs field

$$V(\phi, T) = D(T^2 - T_0^2)\phi^2 - ET\phi^3 + \frac{\lambda_T}{4}\phi^4. \quad (74)$$

The parameters D and E may be expressed in terms of the weak coupling constant $\alpha_W = g^2/4\pi \sim 1/30$ as

$$D \approx \frac{5}{32}g^2, \quad E \approx \frac{g^3}{16\pi}. \quad (75)$$

Here we have used $m_W \approx m_Z \approx m_t$. We can also express the Higgs self-coupling as

$$\lambda_T = g^2 \frac{m_H^2}{8m_W^2}, \quad (76)$$

where m_H is the Higgs mass. This is an effective potential valid near the phase transition temperature where multiple scalar degrees of freedom may be important, and therefore m_H may not be the physical Higgs particle mass [4]. In order to generate a baryon asymmetry which is not washed out in the broken phase, the effective Higgs mass must be $m_H \lesssim 40$ GeV.

In Eq. (74), T_0 is the temperature at which the Higgs mass vanishes and is the lowest temperature for which the high temperature phase is metastable,

$T_0 \sim (m_H/m_W) 250$ GeV. The temperature at which the phase transition nucleates is within the range $T_0 < T < T_c$, where

$$\begin{aligned} \frac{T_c^2 - T_0^2}{T_c^2} &= \frac{E^2}{\lambda_T D} \\ &\approx \frac{\alpha_W}{\pi} \frac{m_W^2}{m_H^2} \\ &\lesssim 0.04. \end{aligned} \tag{77}$$

In terms of these parameters,

$$p_h = aT_h^4 - V(T_h), \tag{78}$$

where $V(T_h)$ is the value of $V(\phi, T_h)$ at its absolute minimum. We can adequately express it as

$$V(T_h) = \varepsilon V_c \tag{79}$$

with

$$\begin{aligned} \varepsilon &= \frac{T_c^2 - T_q^2}{T_c^2 - T_0^2} & V_c &= \frac{1}{2} \frac{E^4}{\lambda^3} T_c^4 \\ &\propto \frac{1}{m_H^{3/2}} & \text{and} & \\ & & & \simeq \frac{2}{\pi} \alpha_W^3 \frac{m_W^6}{m_H^6} T_c^4 \end{aligned} \tag{80}$$

where ε measures the amount of supercooling at the phase transition; it has the value 0.25 for $m_H = 40$ GeV.

The wall thickness δ can conveniently be expressed in terms of V_c and the surface tension $\sigma = \int d\phi \sqrt{2V(\phi, T_c)}$ as

$$\begin{aligned} \delta &= \int_{wall} \frac{d\phi}{\sqrt{2V(\phi, T_c)}} \\ &\simeq \frac{\sigma}{V_c} \sim 10 - 100 \text{ } T^{-1}. \end{aligned} \tag{81}$$

We can now develop an intuition for the scale d_b ($= \sigma/V(T_q)$) which appears naturally in our calculations; from its definition and Eqs. (79) and (81), we can

express it as

$$d_b \simeq \frac{\delta}{\varepsilon}. \quad (82)$$

In the situation of maximal supercooling ($\varepsilon = 1$) $d_b = \delta$ and it increases as the phase transition becomes more weakly first order ($\varepsilon \rightarrow 0$).

According to Eqs. (5) and (78), the relative latent heat is

$$\begin{aligned} \bar{L} &= \frac{8}{2a} \frac{E^2 D}{\lambda_T^2} \left(1 - \frac{E^2}{\lambda_T D} \right) \\ &\approx \frac{5}{2a} \alpha_W^2 \frac{m_W^4}{m_H^4} \\ &\lesssim 0.01. \end{aligned} \quad (83)$$

In the case of $\eta > 1$, we have asserted that there are no unstable perturbations on the basis that perturbations of size larger than the critical wavelength λ_c are stable and that λ_c has the negative value

$$\lambda_c \simeq -\frac{1}{\eta} \frac{4}{\bar{L}} d_b. \quad (84)$$

From Eq. (62), this is a trivial assertion assuming $\bar{L} < 1$ and the ratio d_c/d_b is smaller than one. We now prove the latter assumption. Remembering that d_c is defined as $\sigma/(p_q - p_h)$, and using Eqs. (5) and (14) as well as (79) and (83), this ratio satisfies

$$\frac{d_c}{d_b} = \frac{V(T_q)}{p_q - p_h} < \frac{V_c}{p_q - p_h} \simeq \frac{1}{6v_q} \frac{T_c^2 - T_0^2}{T_c^2} \leq 0.04. \quad (85)$$

To compute the parameter η , we only need to know the temperature dependence of the interface velocity v_b , which is [23,24]

$$v_b \sim \varepsilon = \frac{T_c^2 - T_q^2}{T_c^2 - T_0^2}. \quad (86)$$

The parameter η [Eq. (52)] then becomes

$$\begin{aligned}\eta = -T_{\mathbf{q}} \frac{dv_{\mathbf{b}}}{dT} v_{\mathbf{b}} &\simeq 2 \frac{v_{\mathbf{b}}^2}{\varepsilon} \frac{T_c^2}{T_c^2 - T_0^2} \\ &\simeq \frac{v_{\mathbf{b}}^2}{\varepsilon} \frac{2\pi}{\alpha_W} \frac{m_H^2}{m_W^2}.\end{aligned}\tag{87}$$

As ε behaves parametrically as $m_H^{-3/2}$, we can obtain a lower bound for η by considering the lowest value for m_H , which, to be conservative, we take to be 40 GeV, for which $\varepsilon \sim 0.25$ [23,24]. In such a case,

$$\eta \gtrsim \frac{2\pi}{\alpha_W} v_{\mathbf{b}}^2\tag{88}$$

and unstable perturbations can only develop for

$$v_{\mathbf{b}} \lesssim \sqrt{\frac{\alpha_W}{2\pi}} \sim 0.07,\tag{89}$$

a range clearly not favored by the latest estimates: $0.1 < v_{\mathbf{b}} < 0.9$. From the numerical results above, we find that perturbations on all scales are unable to destabilize the shape of a bubble: if produced spherical, it will stay spherical until it collides with other bubbles and completes the transition. This conclusion, which contradicts a previous analysis [31], is illustrated in Figs. 6a and 6b.

For the QCD quark-hadron transition, the problem is entirely nonperturbative and results are much less clear. \bar{L} is expected to be larger, in the range 0.5–1. In the cosmological context v_b is rather small [25], of the order of 0.04. A fair calculation of η is at present an impossible task. From Eq. (87) we see that unstable perturbations can only develop for

$$v_{\mathbf{b}}^2 < \epsilon \left(1 - \frac{T_0}{T_c}\right) = 1 - \frac{T_{\mathbf{q}}}{T_c}.\tag{90}$$

The standard nucleation analysis for the cosmological phase transition [25], using values of L and σ measured with lattice Monte Carlo techniques [29-30], suggests

$1 - T_q/T_c \approx 0.001$ or an upper limit on v_b of about 0.03. This is very close to the estimated value 0.04 of v_b and thus no definite statement can be made. In terms of the present analysis, QCD, quite interestingly, seems to be a borderline case.

5. Conclusions

The prospect that baryogenesis took place at the electroweak scale has recently been the motivation for the investigations of various aspects of the electroweak phase transition (EWPT). In the present work, we have analyzed the structure of a propagating front separating the unbroken phase from the broken phase. In particular, we have generalized the analysis of Landau [27] of the hydrodynamical stability of a moving front under small perturbations. We have found that, due to the particular nature of the EWPT, this generalization leads to a conclusion opposite to previous works on the subject [31], namely, that *the growth of an electroweak bubble is stable under small perturbations*.

This surprising result comes about because of the intrinsic weakness of the EWPT, which is characterized by the smallness of the ratio of scales d_c/d_b ($\sim \alpha_W$) and by the smallness of the latent heat relative to the energy flowing across the interface $\overline{L} \sim \alpha_W^2 (90/\pi^2 g^*)$, which, in particular, result in a large sensitivity $\eta \sim 1/\alpha_W$ of the velocity of the interface on the temperature of the flowing plasma. In general, there is a *critical velocity* below which instabilities are allowed to develop. In the EW case, we found that this critical velocity is parametrized as $\sim \sqrt{\alpha_W/2\pi} (m_W/m_H)$ and is bounded from above by 0.07. This value is significantly smaller than the values obtained from microscopic calculations [23,24], $0.1 < v_b < 0.9$.

It is interesting to ask under what conditions a smaller value of v_b could be obtained. In the minimal standard model, it would happen [23,24] if the mean free paths ℓ of the gauge bosons and of the top quarks are larger than the thickness of the bubble wall, d_b . The velocity can in such a case reach a value of 0.04

($m_{top} \sim 140$ GeV) and is slightly smaller as the top quark mass increases. In a non-minimal standard model, smaller values might be allowed because of the slight dependence of v_b on the microscopic parameters.

In the QCD phase transition, too little is known to make definite statements on the stability of the quark-hadron interface. One must remember that even the order of the phase transition is not known at present. It is quite interesting that reasonable estimates of the QCD parameters invoked make the cosmological quark-hadron phase transition a borderline case of our stability analysis.

The authors wish to thank the Institute for Theoretical Physics at the University of California, Santa Barbara, where this work was begun.

REFERENCES

1. D. A. Kirzhnits and A. Linde, *Ann. Phys.* **101**, 195 (1976).
2. D. Anderson and L. Hall, *Phys. Rev.* **D45**, 2682 (1992).
3. M. Carrington, *Phys. Rev.* **D45**, 2933 (1992).
4. M. Dine, R.G. Leigh, P. Huet, A. Linde, and D. Linde, *Phys. Lett.* **B283**, 319 (1992).
5. M.E. Shaposhnikov, *JETP Lett.* **44**, 465 (1986);
Nucl. Phys. **B287**, 757 (1987); **B299**, 797 (1988);
A.I. Bochkarev, S.Yu. Khlebnikov and M.E. Shaposhnikov,
Nucl. Phys. **B329**, 493 (1990).
6. L. McLerran, *Phys. Rev. Lett.* **62**, 1075 (1989).
7. N. Turok and J. Zadrozny, *Phys. Rev. Lett.* **65**, 2331 (1990); *Nuc. Phys.* **B358**, 471 (1991).
8. L. McLerran, M. Shaposhnikov, N. Turok and M. Voloshin, *Phys. Lett.* **B256**, 561 (1991).

9. M. Dine, P. Huet, R. Singleton and L. Susskind, *Phys. Lett.* **B257**, 351 (1991).
10. A.D. Sakharov, *Pisma ZhETF* **5**, 32 (1967).
11. G. 't Hooft, *Phys. Rev. Lett.* **37**, 8 (1976); *Phys. Rev.* **D14**, 3432, (1976).
12. A. Linde, *Phys. Lett.* **70B**, 306 (1977).
13. V.A. Kuzmin, V.A. Rubakov and M.E. Shaposhnikov, *Phys. Lett.* **B155**, 36 (1985).
14. P. Arnold and L. McLerran, *Phys. Rev.* **D36**, 581, (1987); **D37**, 1020 (1988).
15. L. Carson, Xu Li, L. McLerran and R. T. Wang, *Phys. Rev.* **D42**, 2127 (1990).
16. J. Ambjorn, M. Laursen and M. Shaposhnikov, *Phys. Lett.* **197B**, 49, (1989); *Nucl. Phys.* **B316**, 483 (1990); J. Ambjorn, T. Askgaard, H. Porter and M. Shaposhnikov, *Phys. Lett.* **B244**, 479 (1990); *Nucl. Phys.* **B353**, 346 (1991).
17. For a review see for example D. Toussaint, *Nucl. Phys. B[Proc. Suppl.]* **26**, 3 (1992).
18. F. Wilczek, *Int. J. Mod. Phys.* **A7**, 3911 (1992); R. Pisarski and F. Wilczek, *Phys. Rev.* **D29**, 338 (1984).
19. P. Steinhardt, *Phys. Rev.* **D25**, 2074 (1982).
20. M. Gyulassy, K. Kajantie, H. Kurki-Suonio and L. McLerran, *Nucl. Phys.* **B237**, 477 (1984).
21. H. Kurki-Suonio, *Nucl. Phys.* **B255**, 231 (1985).
22. K. Enqvist, J. Ignatius, K. Kajantie and K. Rummukainen, *Phys. Rev.* **D45**, 3415 (1992).
23. M. Dine, R. G. Leigh, P. Huet, A. Linde and D. Linde, *Phys. Rev.* **D46**, 550 (1992).
24. B. H. Liu, L. McLerran and N. Turok, TPI-MINN-92-18-T.

25. K. Kajantie, *Phys. Lett.* **284B**, 331 (1992).
26. B. Link, *Phys. Rev. Lett.* **68**, 2425 (1992).
27. L. Landau, *Acta Physicochimica URSS*, **XIX**, No. 1 (1944); L. D. Landau and E. M. Lifshitz, *Fluid Mechanics*, §128, (Pergamon Press, Oxford, 1987).
28. V. M. Kontorovich, *Soviet Physics JETP* **34**, 127 (1958).
29. K. Kajantie, L. Kärkkäinen and K. Rummukainen, *Nucl. Phys.* **B357**, 693 (1991).
30. S. Huang, J. Potvin, C. Rebbi and S. Sanielevici, *Phys. Rev.* **D42**, 2864 (1990).
31. P. Kamionkowski and K. Freese, U.C. Berkeley Preprint CFPA-TH-92-17.
32. K. Freese and F. Adams, *Phys. Rev. D* **41**, 2449 (1990).

Figure Captions

Figure 1: The burning front in the rest frame of the front. The wall is moving to the left, the inflowing velocity of the high temperature phase is v_q and the outflowing velocity of the low temperature phase is v_h . Deflagrations are when $v_q < v_h$ and detonations when $v_q > v_h$.

Figure 2: Structure of a detonation bubble in 1+1-dimensions: (a) The time dependence of the $x > 0$ part of the bubble with the three fronts demanded by the boundary conditions. The dotted line shows the path of a fluid element. (b) The energy density and flow rapidity of matter as functions of space-time rapidity $y = \tanh^{-1}(x/t)$ for a detonation bubble. For Jouguet detonations $y_1 = y_s$ and no region of constant velocity appears. The magnitudes of the quantities shown are related by Eqs. (17)–(20).

Figure 3: Structure of a deflagration bubble in 1+1-dimensions: (a) The time dependence of the $x > 0$ part of the bubble with the two fronts demanded by the

boundary conditions. The dotted line shows the path of a fluid element. (b) The energy density and flow rapidity of matter as functions of x/t for a deflagration bubble. The magnitudes of the quantities shown are related by Eqs. (14)–(16).

Figure 4: Regions allowed by the continuity of energy and momentum fluxes and entropy increase for combustion from a high T phase at $T = T_1$ to low T phase at $T = T_0$. The three approximately linear boundaries follow for $T_1 - T_c, T_0 - T_c \ll T_c$ from Eqs. (12) by demanding the velocities to be real and from the second of Eqs. (13). The curves $v_{\text{def}} = \text{const.}$ are explicitly given by Eqs. (14) and (15). Note that detonations are possible only after supercooling by at least $\bar{L}/4$. Horizontal hatching corresponds to the forbidden region characterized by $\Delta s < 0$, and vertical hatching to imaginary velocity.

Figure 5: A plot of the dispersion relation (36) for (a) $v < c_s$, (b) $v > c_s$.

Figure 6: Long wavelength limit of Ω/k computed for the electroweak theory ($m_h = 60$ GeV). (a) Landau's results (21) (dashed curve) and our results (63) (solid curve) are shown for small velocities $v \ll c_s$. (b) In the limit $v \rightarrow c_s$, the inadequacy of (21) and (63) is illustrated by comparison with our general formula (70) (dotted curve).

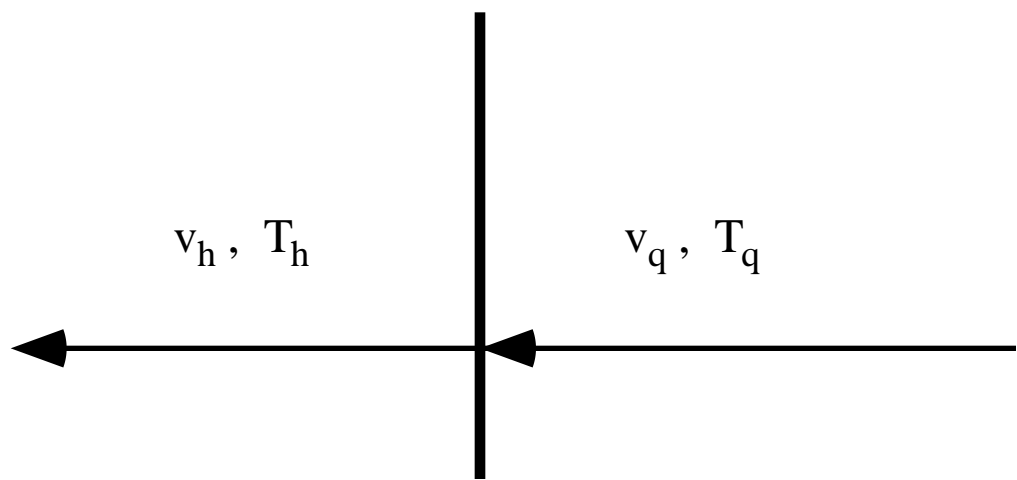


Fig. 1

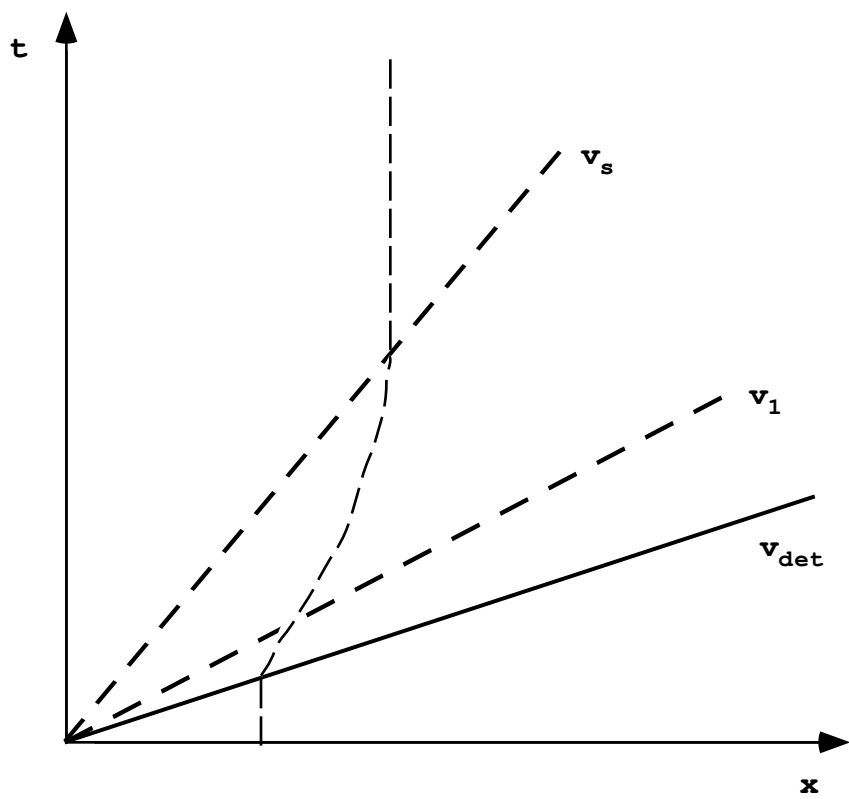


Fig. 2(a)

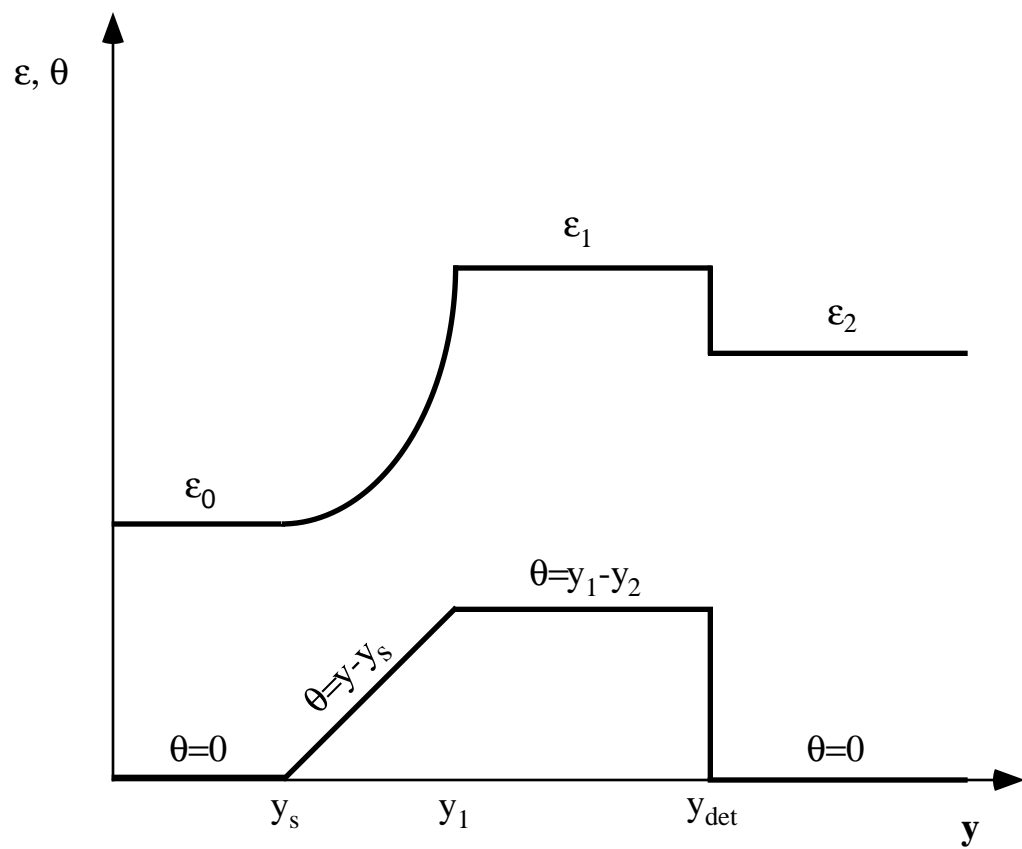


Fig. 2(b)

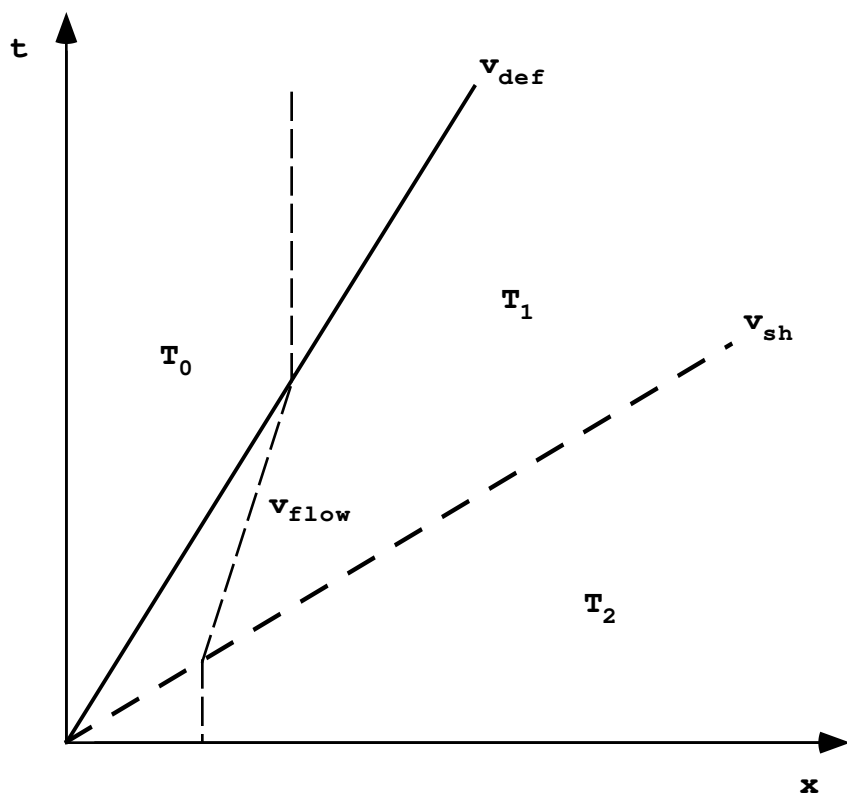


Fig. 3(a)

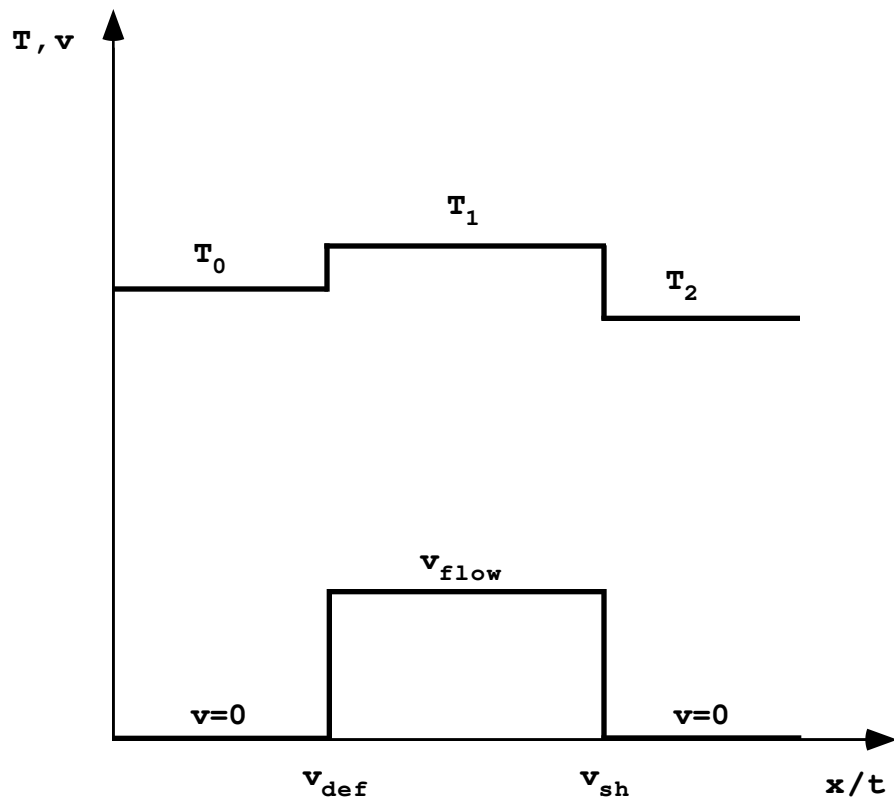


Fig. 3(b)

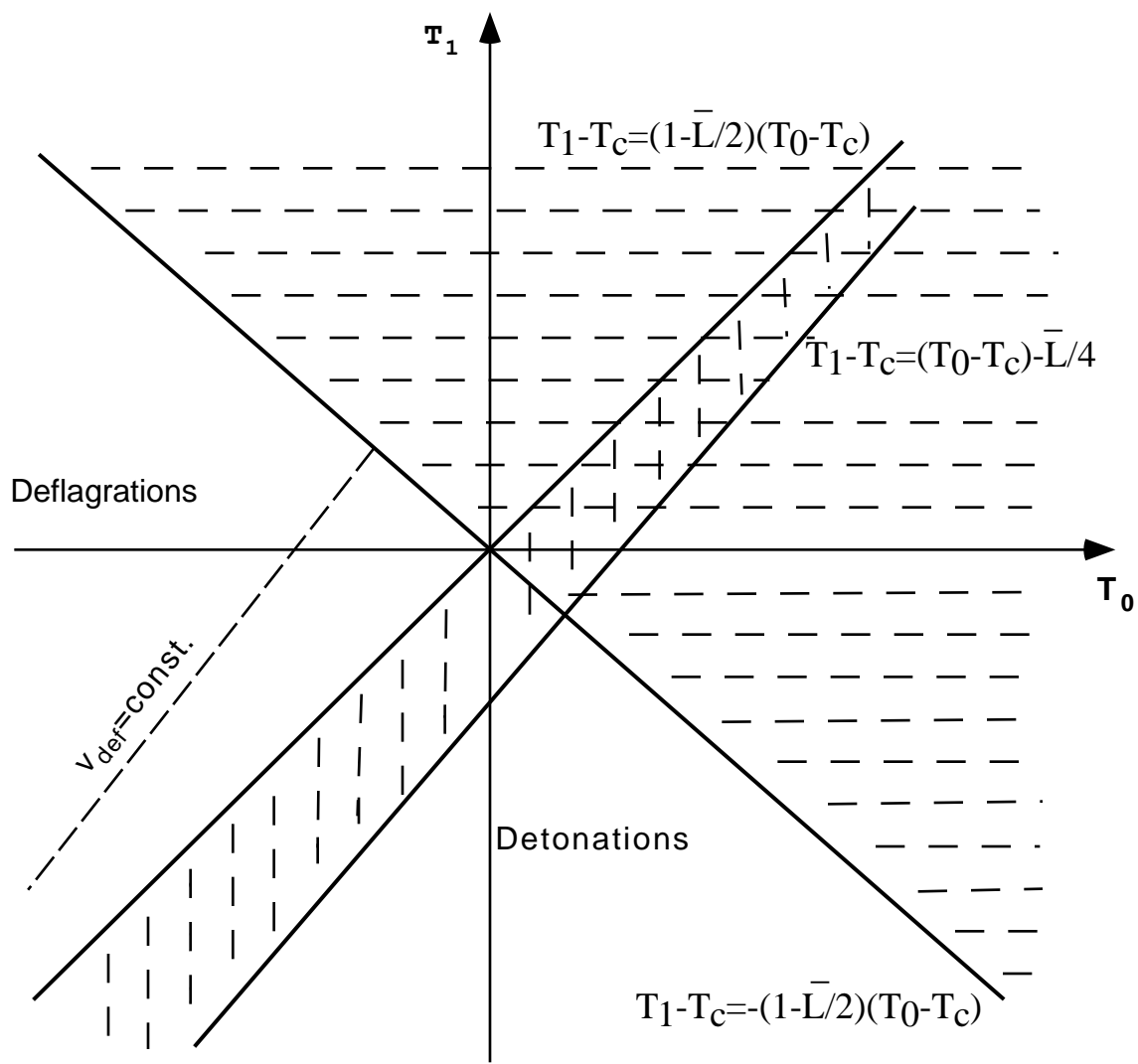


Fig. 4

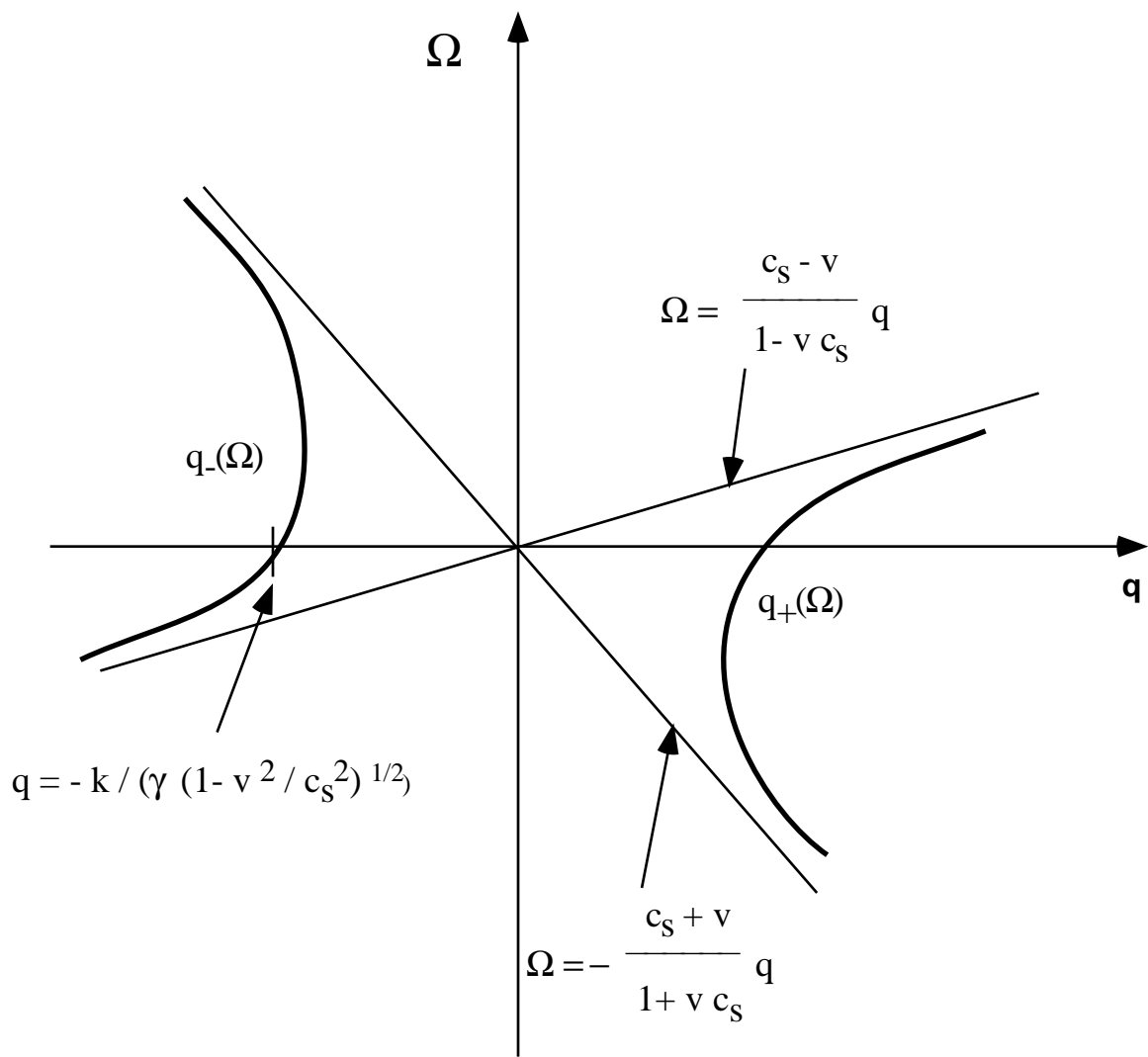


Fig. 5(a)

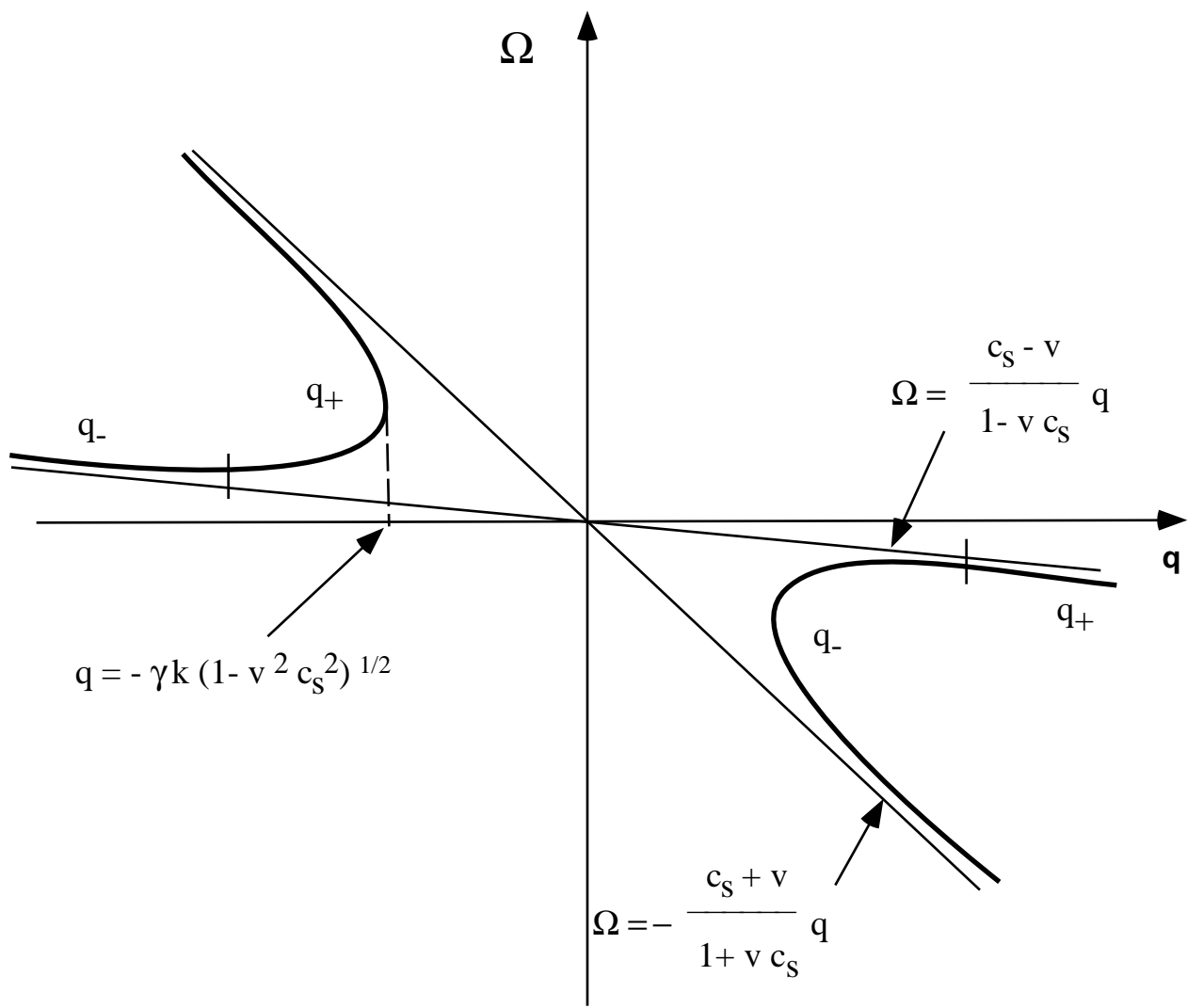


Fig. 5(b)

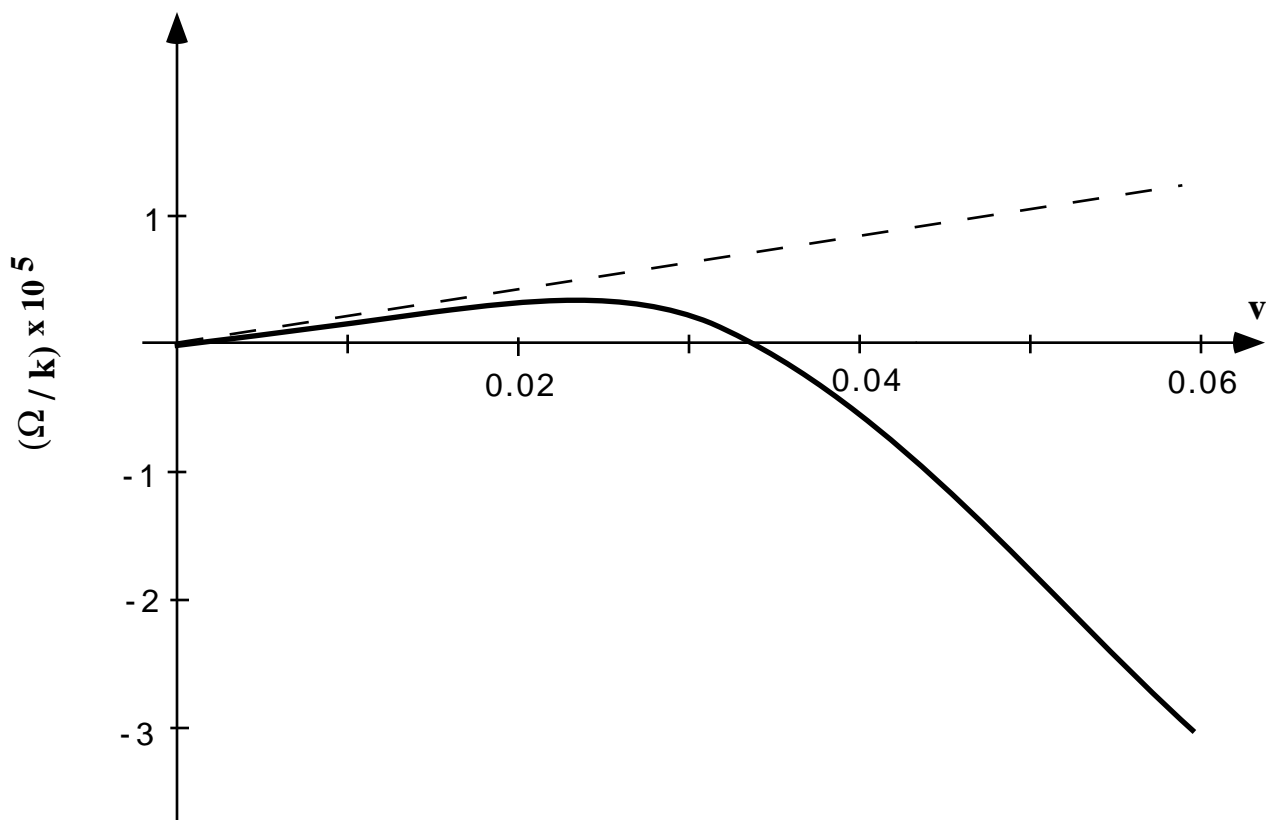


Fig. 6(a)

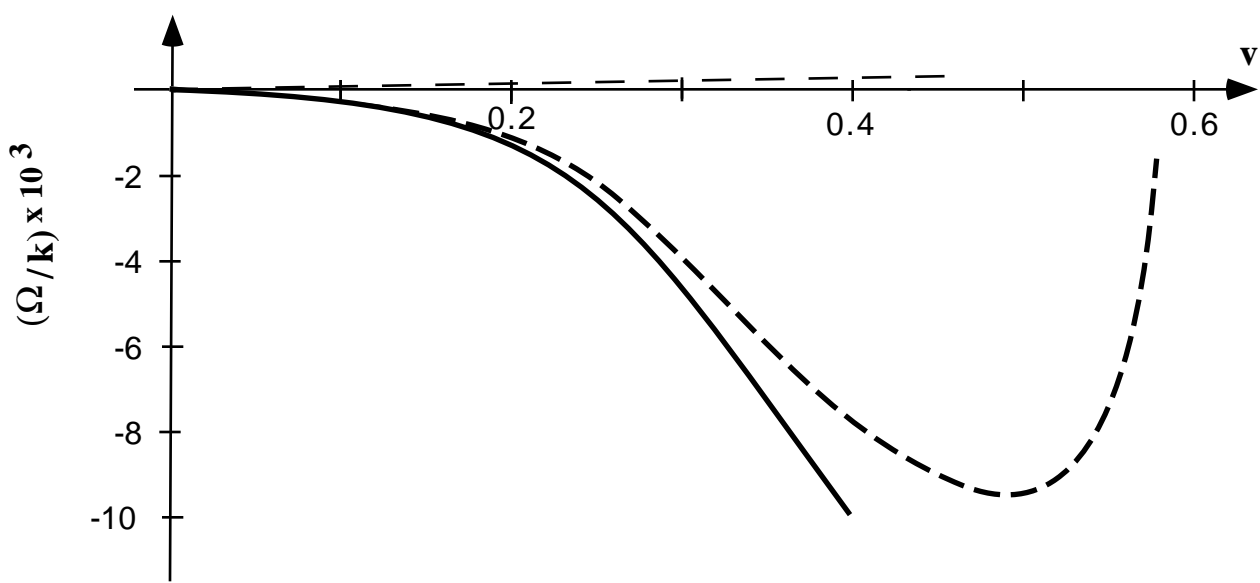


Fig. 6(b)